Free Radical Biology and Medicine 138 (2019) 23–32

Contents lists available at ScienceDirect

Free Radical Biology and Medicine

journal homepage: www.elsevier.com/locate/freeradbiomed

Original article

Early induction of senescence and immortalization in PGC-1α-deficient mouse embryonic fibroblasts

Ignacio Prieto[a], Alberto Zambrano[b], Javier Laso[c,1], Ana Aranda[a], Enrique Samper[d], María Monsalve[a,*]

[a] Instituto de Investigaciones Biomédicas "Alberto Sols" (CSIC-UAM). Arturo Duperier 4. 28029, Madrid, Spain
[b] Unidad Funcional de Investigación en Enfermedades Crónicas (UFIEC), Instituto de Salud Carlos III. Ctra. Majadahonda-Pozuelo km 2. 28220, Madrid, Spain
[c] Fundación Centro Nacional de Investigaciones Cardiovasculares Carlos III (CNIC). Melchor Fernández Almagro 3, 28029, Madrid, Spain
[d] NIMGenetics, Genómica y Medicina S.L. Faraday, 7. 28049, Madrid, Spain

ARTICLE INFO

Keywords:
Mitochondria
Oxidative stress
PGC-1α
Senescence
Immortalization

ABSTRACT

Aims: Oxidative stress is known to induce early replicative senescence. Senescence has been proposed to work as a barrier to immortalization and tumor development. Here, we aimed to evaluate the impact of the loss of peroxisome proliferator activated receptor γ co-activator 1α (PGC-1α), a master regulator of oxidative metabolism and mitochondrial reactive oxygen species (ROS) generation, on replicative senescence and immortalization in mouse embryonic fibroblasts (MEFs).

Results: We found that primary MEFs lacking PGC-1α showed higher levels of ROS than wild-type MEFs at all cell passages tested. The elevated production of ROS was associated with higher levels of oxidative DNA damage and the increased formation of DNA double-strand breaks. Evaluation of the induction of DNA repair systems in response to γ-radiation indicated that the loss of PGC-1α also resulted in a small but significant reduction in their activity. DNA damage induced the early activation of senescence markers, including an increase in the number of β-galactosidase-positive cells, the induction of p53 phosphorylation, and the increase in p16 and p19 protein. These changes were, however, not sufficient to reduce proliferation rates of PGC-1α-deficient MEFs at any cell passage tested. Moreover, PGC-1α-deficient cells escaped replicative senescence.

Innovation & conclusion: PGC-1α plays an important role in the control of cellular senescence and immortalization.

1. Introduction

Cellular senescence was first described as the state of a stable long-term loss of replicative capacity resulting from prolonged replication of cells in culture [1]. This form of senescence, termed replicative senescence, occurs in cultured human cells that reach an intolerable telomeric shortening [2], while in mouse embryonic fibroblasts (MEFs) it is independent of telomeres and more closely recapitulates the accelerated or premature senescence of human cells following genotoxic stress or oncogene activation, termed "stress-induced premature senescence" and "oncogene-induced senescence", respectively [3,4].

Senescence is ultimately driven by DNA damage [5]. Previous studies in MEFs have shown that both exogenously added ROS and elevated endogenous ROS production induces early senescence [6,7]. Partial deficiency of *sod 2*, encoding for mitochondrial manganese superoxide dismutase (MnSOD), induces mitochondrial oxidative stress and leads to an increase in DNA double-strand breaks (DSBs), end-to-end chromosome fusions, chromosomal translocations, and also loss of cell viability and proliferative capacity, indicating that mitochondrial oxidative stress can induce genomic instability and therefore have a profound effect on cancer and aging [8]. Conversely, decreasing endogenous ROS levels with the mitochondria-targeted antioxidant MitoQ delays replicative senescence [9].

Regardless of the signals that induce senescence, two major tumor suppressor pathways, p53-p21WAF1 and pRb-p16INK4a, are key to control the execution and maintenance of this response [10,11]. In murine cells, the ARF-p53 pathway has a dominant role, whereas in human cells pRb-p16INK4a seems to be at least equally critical [12].

* Corresponding author. Instituto de Investigaciones Biomédicas "Alberto Sols" (CSIC-UAM), Arturo Duperier 4, Room 1.3.2, 28029, Madrid, Spain.
E-mail addresses: nprieto58@gmail.com (I. Prieto), azambra@isciii.es (A. Zambrano), jlaso@lrc.es (J. Laso), aaranda@iib.uam.es (A. Aranda), esamper@nimgenetics.com (E. Samper), mpmonsalve@iib.uam.es (M. Monsalve).
[1] Present Address: Laboratori de Referència de Catalunya. de la Selva 10, El Prat de Llobregat, 08820-Barcelona (Spain).

https://doi.org/10.1016/j.freeradbiomed.2019.04.015
Received 3 December 2018; Received in revised form 10 April 2019; Accepted 13 April 2019
Available online 25 April 2019

Both p53 and the cyclin-dependent kinase (CDK) inhibitor p16 are activated in response to elevated ROS [13,14]. It has been proposed that a positive feedback loop of mitochondrial damage, ROS production, and DNA damage repair (DDR) by the activation of p53 is required for the establishment of the growth arrest phenotype during cellular senescence [13]. The steady increase in ROS production by this positive feedback loop is thought to replenish short-lived DNA damage *foci* and to maintain an ongoing DDR, which are believed to be both necessary and sufficient to establish and sustain the senescence phenotype [15]. The p16 pathway can also promote a ROS-dependent positive feedback loop, which reinforces the irreversible cell cycle arrest in senescent cells, partly through the downregulation of large tumor suppressor kinase 1, a kinase required for cytokinesis [16].

In the last years, several studies have supported a role for cellular senescence as a natural barrier to tumor development [17,18]. Such studies include the findings that p53-driven senescence in mouse models can limit cancer progression in existing malignancies [19]. This concept has led to the proposal that inducing cellular senescence, including treatments that elevate intracellular ROS levels, can be of therapeutic utility in cancer. The demonstration that cancer cells can respond to therapeutic agents both *in vivo* and *in vitro* by inducing a senescence phenotype has been encouraging. However, the safety of these approaches is still a matter of debate mainly because senescent cells become resistant to induced apoptotic cell death and senescence could be a reversible process [20].

PGC-1α is a transcriptional coactivator that controls the expression of most, if not all, of the metabolic pathways that allow cellular adaptation to limited nutrient availability or to increased metabolic demand (e.g., cold exposure and exercise) [21]. Moreover, PGC-1α boosts the catabolic and oxidative capacity of the cell, and coordinately induces the expression of a suite of antioxidant enzymes that prevents oxidative damage under these conditions [22]. As a result of PGC-1α induction, cells present an enhanced antioxidant capacity and a net reduction in ROS levels. Obesity and metabolic syndrome are normally associated with a decrease in PGC-1α activity in all the tissues and cell types where it has been investigated [23–27]. It has been suggested that PGC-1α down regulation may be involved in the early aging associated with metabolic dysfunction. Additionally, PGC-1α has been shown to interact and regulate p53 activity [28] and its absence can promote telomere shortening and vascular senescence [29,30] at least in part through TERT down-regulation [31]. Along this line, recent studies indicate that reduced PGC-1α levels can be a relevant factor in tumor development. It particular, its downregulation has been associated with the induction of c-Myc, a master regulator of cell proliferation [32]. Moreover, a recent whole-genome expression analysis of PGC-1α$^{+/+}$ and PGC-1α$^{-/-}$ hepatocytes showed that cancer and cell cycle were among the major functional pathways regulated by PGC-1α [31].

In the present study, we aimed to elucidate the role of PGC-1α in ROS-induced cellular senescence and immortalization using serially-passaged primary MEFs as a model system. We found that loss of PGC-1α resulted in elevated mitochondrial ROS production, increased oxidative DNA damage, genomic instability and the induction of senescence mediators including p53 and p16. However, these changes did not result in a reduction in cell proliferation. Importantly, MEFs lacking PGC-1α efficiently escaped senescence and were immortalized.

2. Materials and methods

2.1. Cell culture

Wild-type and PGC-1α-deficient MEFs were isolated and cultured as previously described [33]. Eight embryos from 3 PGC-1α$^{+/+}$ litters and 8 from 3 PGC-1α$^{-/-}$ litters were used to prepare MEF cultures (8 of each). MEFs (10^6) were seeded in 100-cm^2 dishes and cultured in Dulbecco's modified Eagle's medium (Sigma) with 10% fetal bovine serum and antibiotics. Cells were passaged every 72 h, counted using a hemocytometer and re-seeded at 10^6 cells/dish. This process was repeated until the cultures reached senescence. Growth rates were calculated with the formula $\Delta Growth = \log_2 (n_f\text{-}n_i)$, where n_i is the initial cell number and n_f is the final cell number [8]. When cultures escaped senescence and immortalized, cells were counted and seeded again for 5 additional passages to determine post-immortalization growth rates.

The procedures used conformed to the Declaration of Helsinki. All animals received humane care according to the criteria outlined in the "Guide for the Care and Use of Laboratory Animals" prepared by the National Academy of Sciences and published by the National Institutes of Health (No. 86–23 revised 1985). Animal experimental protocols were approved by the CSIC Ethic's Committee (SAF2012-37693, 333/2015) and the Consejería de Medio Ambiente of the Comunidad de Madrid (PROEX 317/15).

2.2. Irradiation

Cell cultures plated in 8-well chamber slides (Nunc) were exposed to 3 Gy gamma irradiation using an irradiator (J.L. Shepherd Mark 1, San Fernando, CA).

2.3. Labeling of DNA breaks

Procedures were as previously described [34]. Briefly, cells were incubated with biotin-11-dUTP (Thermo Scientific) in the presence of terminal deoxy-transferase (TdT) (BioLabs). Cells were then incubated with an anti-biotin-HRP-conjugated antibody (Sigma), and the labeled breaks were revealed using the DAB system (Vector Lab). Nuclei were stained with Nuclear Fast Red (Sigma). Photographs were taken with Nikon E90i (Nikon) microscope using a DS-Fi1 camera and analyzed using the NES Elements software (Nikon).

2.4. Immunofluorescence

Cell fixation, staining and analysis procedures were as previously described [34]. The following antibodies were used: γH2AX (05–636, Millipore), TP53BP1 (NB100-304, Novus Biologicals) and 8-OH-deoxyguanosine (8-OH-dG) (NB600-1508, Novus Biologicals). Images were acquired with Nikon E90i microscope using a DS-Q1 camera and analyzed with the NES Elements software. 100 cells were analyzed from 5 to 10 different fields in 3 independent experiments.

2.5. Mitochondrial superoxide detection

Mitochondrial superoxide was evaluated by labeling cells with MitoSOX Red as described [35,36]. Images were acquired using the LSM710 spectral confocal microscope (Zeiss).

2.6. β-galactosidase activity

Evaluation of senescence-associated β-gal (SA-β-gal) activity was performed at pH 6 as previously described [1]. Differential interference contrast images were acquired using a Nikon E90i microscope with a DS-Fi1 camera and analyzed using the NES Elements software.

2.7. Protein extraction and western blotting

Whole cell extracts were prepared as previously described [37]. Proteins were separated using 12% SDS-PAGE gels and transferred to PVDF Hybond-P membranes (Amersham/GE healthcare) by semidry transference using the TransBlot SD cell system (Bio-Rad). The following antibodies were used: p53 (sc-126, Santa Cruz), Ph-p53 (9286), AMPK (2532) and phospho-AMPK (2535), all from Cell Signaling Technology, p16 (sc-1207, Santa Cruz), MnSOD (ADI-SOD-110, Enzo Life Sciences), p19 (R562, Abcam), cyt C (556433, BD Biosciences), and β-actin (A5441, Sigma). ImageJ software (NIH) was used to measure and analyze protein band intensity.

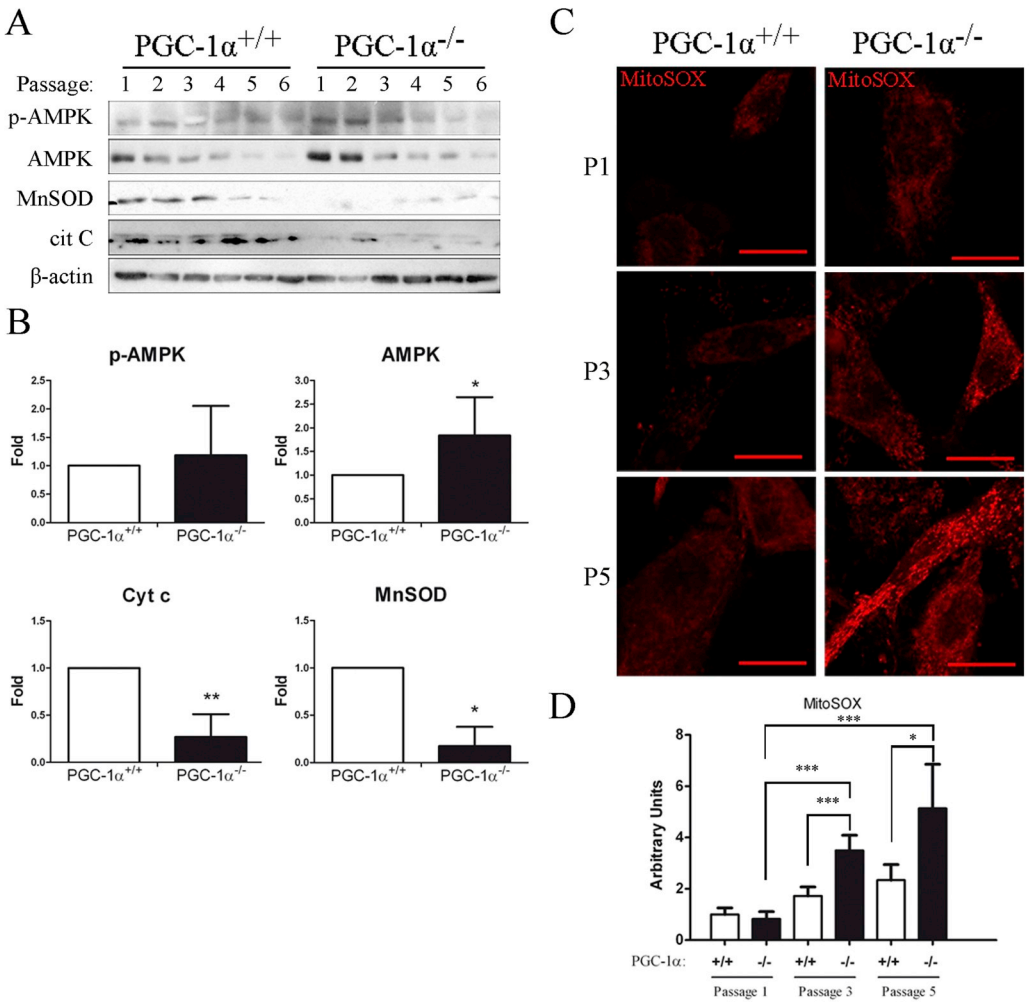

Fig. 1. PGC-1α-deficient MEFs show reduced levels of MnSOD and elevated levels of superoxide. **A)** Western blot analysis of cyt *c*, MnSOD and AMPK (total and phosphorylated) in serially-passed PGC-1α$^{+/+}$ and PGC-1α$^{-/-}$ MEFs. β-actin was used as a loading control. Panel shows a representative western blot. **B)** Graphs show the quantitative analysis of the protein expression levels relative to those in PGC-1α$^{+/+}$ MEFs, assigned a value of 1. Data represent means ± SD of passages 1–6. **C)** Confocal microscopy images of MitoSOX™ Red staining (40 ×) of PGC-1α$^{+/+}$ and PGC-1α$^{-/-}$ MEFs at passage 1 (p1), p3 and p5. Scale bar, 20 μm. **D)** Quantitative analysis of MitoSOX™ Red images. Data represent the means ± SD, n = 4 independent cell cultures. *p < 0.05; **, p ≤ 0.01; ***, p ≤ 0.005.

2.8. RNA isolation and quantitative reverse transcription polymerase chain reaction

Total mRNA was extracted using TRI Reagent (Sigma) and retro-transcribed with reverse transcriptase (M-MLV RT enzyme; Invitrogen). The resulting cDNA was analyzed by qPCR using a SyBr Green Master Mix (Applied Biosystems) and an Eppendorf MasterCycler RealPlex (Eppendorf). The following primer sets were used:

Primers	Sequence 5′-3′
Forward-SESN1	CAGGAAATGCTTCGGTAAGTG
Reverse-SESN1	GTAACTTCATCATCGTCCGA
Forward -SESN2	CCACTCTCTGGCCTCCTTTG
Reverse -SESN2	TTCAAAGCCCCCTGAGTTGT
Forward —BBC3	GTACGAGCGGCGGAGACAAG
Reverse —BBC3	CTAGTTGGGCTCCATTTCTGG
Forward -BAX	TTTGCTACAGGGTTTCATCC
Reverse -BAX	CCACGTCAGCAATCATCCT
Forward -PMAIP1	GCAGAGCTACCACCTGAGTT
Reverse -PMAIP1	GAGTTGAGCACACTCGTCCT
Forward -GLS2	AGCTCTTCCAAAAGTGTGTG
Reverse -GLS2	GGATGTAGGCTGCCACTTTG
Forward -ALDH4	TGAAGGTGACCAATGAGCCC
Reverse -ALDH4	GTGCATGGTTAAAGGGCGAC
Forward -PARK2	TGCACAGATGTCAGGAGCCC
Reverse -PARK2	CCTGTTGTACTGCTCTTCTCCA
Forward -NDN	AAGAAGGCCCTGGAGAGTTA
Reverse -NDN	TATTTATGGTGGGGTTGCAT
Forward -GADD45A	CGTAGACCCCGATAACGTGG
Reverse -GADD45A	TTCGTCACCAGCACACAGTG
Forward –p16	GTC GCA GGT TCT TGG TCA CT
Reverse –p16	CGA ATC TGC ACC GTA GTT GA
Forward –p19	CCA CCG GTA TCC ACT ATG CT
Reverse –p19	TCA GGA GCT CCA AAG CAA CT
Forward –p21	GTA CTT CCT CTG CCC TGC TG
Reverse –p21	TCT GCG CTT GGA GTG ATA GA
Forward -TERC	GCTGTGGGTTCTGGTCTTTTGTTC
Reverse -TERC	CGTTTGTTTTTGAGGCTCGGG

Statistics. Several passages were group together for analytical purposes to compare “early” and “late” passages when values within the rage did not differ significantly per passage. However, since as for each marker and determination type this is not a constant, we refrained from defining them as early and late. Data are expressed as means ± SD. Statistical significance was evaluated by one-way analysis of variance or two-tailed upaired *t* test. Values were considered statistically significant at p ≤ 0.05.

3. Results

3.1. Enhanced mitochondrial ROS production in serially passaged primary PGC-1α-deficient MEFs

To evaluate the role of PGC-1α in cellular senescence, we used the classical 3T3 protocol [38] to establish the growth and immortalization time of eight individual PGC-1α$^{+/+}$ and eight PGC-1α$^{-/-}$ MEF cultures under standard culture conditions of 5% CO_2, 20% O_2 and 37 °C. These cultures were then used for further analysis. PGC-1α levels could be detected by western blot in PGC-1α$^{+/+}$ MEFs but not in PGC-1α$^{-/-}$ MEF (Supp. Fig. 1).

We previously showed that PGC-1α positively regulates the expression of antioxidant genes, and its deficiency results in elevated mitochondrial ROS levels in various mouse primary cell types, including vascular endothelial cells, hepatocytes and MEFs [33]. We used western blotting at different cell passages to analyze the impact of PGC-1α deficiency on two of its targets cytochrome *c* (cyt *c*), a component of the mitochondrial electron transport chain, and MnSOD, a key mitochondrial detoxification enzyme. As anticipated, protein levels of cyt *c* and MnSOD at cell passage (p)1 were lower in PGC-1α$^{-/-}$ MEFs than in PGC-1α$^{+/+}$ MEFs (Fig. 1A). Serial cell passaging led to a robust reduction in MnSOD levels in PGC-1α$^{+/+}$ MEFs, while this was less evident in PGC-1α$^{-/-}$ MEFs (Fig. 1A and B), suggesting that MnSOD downregulation was at least partially attributable to PGC-1α activity. Consistently, PGC-1α levels were reduced in late passages (Supp. Fig. 2). By contrast, cyt *c* levels remained relatively stable over continuous passage. To evaluate whether PGC-1α$^{-/-}$ MEFs were metabolically compromised, we measured the phosphorylation status of the cellular energy sensor AMPK as an indicator of metabolic stress. Results showed that whereas total AMPK levels where significantly higher in PGC-1α$^{-/-}$ MEFs, the AMPK phosphorylation/AMPK total ratio was not significantly affected by the lack of PGC-1α across cell passages or when passages 1–3 and 4–6 were analyzed separately (Fig. 1A–B, Supp. Fig. 3).

We next used MitoSOX Red staining to evaluate the effect of serial passage on the levels of mitochondrial superoxide (O_2^-). MitoSOX labeling increased with cell passage in both PGC-1α$^{+/+}$ and PGC-1α$^{-/-}$ MEFs (Fig. 1C and D). Although not different at early passage (p1), MitoSOX fluorescence became higher in PGC-1α$^{-/-}$ MEFs than in PGC-1α$^{+/+}$ MEFs upon serial passaging and this was more prominent at later passages (Fig. 1C and D). This result suggested a synergistic effect of PGC-1α-dependent mitochondrial dysfunction on passage-induced oxidative stress.

3.2. Deficiency of PGC-1α leads to an increase in oxidative DNA damage and the generation of DNA double-strand breaks

Given that oxidative stress can result in oxidative DNA damage, we next evaluated the formation of 8-oxo-deoxyguanosine (8-OH-dG), a major biomarker of ROS-dependent DNA oxidation [34]. Quantification of the number of 8-OH-dG-containing nuclear *foci* in p2 and p5 MEFs by immunofluorescence staining with a specific antibody showed that while the number of *foci* in p2 PGC-1α$^{+/+}$ and PGC-1α$^{-/-}$ MEFs was not significantly different, the number of positive *foci* in PGC-1α$^{-/-}$ MEFs at p5 increased dramatically and was significantly higher than that in PGC-1α$^{+/+}$ MEFs (Fig. 2A and B). Colocalization of 8-OH-dG nuclear *foci* and TP53BP1, a protein that is present in DNA damage repair (DDR) complexes, was used as a control for specificity.

ROS generation is linked to the formation of DNA strand breakage. ROS that are produced primarily by mitochondria can provoke base oxidation, abasic sites, and both DNA single and DSBs [39,40]. Moreover, a significant number of the DNA single-stranded lesions induced by ROS are converted into DSBs, either by a direct mechanism or by the repair process itself [41]. We therefore next evaluated the impact of the elevated levels of ROS-induced DNA oxidation on the formation of DSBs. To do this, we carried out a cytochemical analysis using the specific activity of terminal transferase (TdT) to incorporate biotin-11-dUTP into the 3′-end of the DNA chain [34]. We observed that at p4, the number of cells with DNA breaks was significantly higher in PGC-1α$^{-/-}$ MEFs than in PGC-1α$^{+/+}$ MEFs (40% and 78% in PGC-1α$^{+/+}$ and PGC-1α$^{-/-}$ MEFs, respectively) (Fig. 2C and D), suggesting that the higher levels of oxidized DNA in PGC-1α$^{-/-}$ cells had a significant impact on genomic instability.

Of the different types of DNA lesions formed by oxidation, DSBs are the most deleterious, and are potent inducers of chromosomal rearrangements such as deletions, translocations or amplifications [42]. The phosphorylated histone, H2AFX (γH2AFX), and TP53BP1 are sensitive markers of DNA damage [43,44]. When DSBs are detected, a signaling cascade is initiated by the phosphorylation of H2AFX by ataxia-telangiectasia mutated kinase near the break site, followed by the rapid recruitment of TP53BP1 to the chromatin surrounding the DNA lesion. Among other functions, TP53BP1 acts as a molecular scaffold in damaged chromatin during non-homologous end-joining repair mechanism [45].

We therefore determined the formation of nuclear DNA damage *foci* containing DSB repair complexes by examining for colocalization of γH2AFX and TP53BP1, part of the DNA repair complex [34]. We noted a good colocalization of both DDR markers. Representative immunofluorescence images of the individual signals can be found in Supp. Fig. 4, and the quantitative evaluation of their linear correlation in Supp. Fig. 5. Both PGC-1α$^{+/+}$ and PGC-1α$^{-/-}$ MEFs showed higher number of cells with DNA damage *foci* at p5 than at p2 (Fig. 2E and F). Additionally, the number of DNA damage *foci* was significantly higher in PGC-1α$^{-/-}$ MEFs than in PGC-1α$^{+/+}$ MEFs both at p2 and p5 (Fig. 2E and F).

3.3. PGC-1α-deficient MEFs have reduced DNA damage repair activity

The elevated levels of DSBs observed in PGC-1α$^{-/-}$ MEFs could result from the observed increase in oxidative DNA damage but also to other factors, in particular, a reduced capacity for DNA repair. To test this, we evaluated the effect of PGC-1α deficiency for the reversal of DNA damage. Thus, PGC-1α$^{+/+}$ and PGC-1α$^{-/-}$ MEFs at p2 were exposed to 3 Gy irradiation and the number of γH2AFX nuclear *foci* was analyzed at different time points, from 15 min to 9 h post-irradiation. Image quantitation revealed that at 15 min post-irradiation, 100% of PGC-1α$^{+/+}$ and PGC-1α$^{-/-}$ MEFs showed nuclear *foci*, and the number of cells with more than 10 *foci* per nucleus was quite similar (over 90%) in both cell types, suggesting that the extent of damage was comparable (Fig. 3A–C). The total number of cells with more than 10 nuclear *foci* had dropped significantly at 3 h both in PGC-1α$^{+/+}$ and PGC-1α$^{-/-}$ MEFs, and the trend continued until 24 h, when levels reached a steady-state. Notably, at all stages post-irradiation, the number of cells with more than 10 nuclear *foci* was consistently higher in PGC-1α$^{-/-}$ MEFs than in PGC-1α$^{+/+}$ MEFs (Fig. 3A–C). This result suggests that PGC-1α$^{-/-}$ MEFs have an impaired DNA repair system. However, since the maximal difference between the two cell types, occurring at 3 h post-irradiation, represented less than 10% of the total number of cells, it seems unlikely that this partial deficiency could play a major role in the enhanced accumulation of DSBs in serially passaged PGC-1α$^{-/-}$ MEFs.

Induction of the DNA damage response was also evaluated in serially passage cells by testing the levels of TLS, a downstream mediator of ATM [60], we found that TLS levels tended to be lower in PGC-1α$^{-/-}$ MEFs but differences did not reach statistical significance (Supp. Fig. 6).

3.4. Early induction of senescence in PGC-1α-deficient MEFs

Elevated ROS levels and DNA damage can independently or cooperatively induce cellular senescence [46]. Therefore, we next evaluated the induction of senescence-associated β-galactosidase (SA-β-gal) activity at pH 6 as a metric of senescence. The absolute numbers of β-

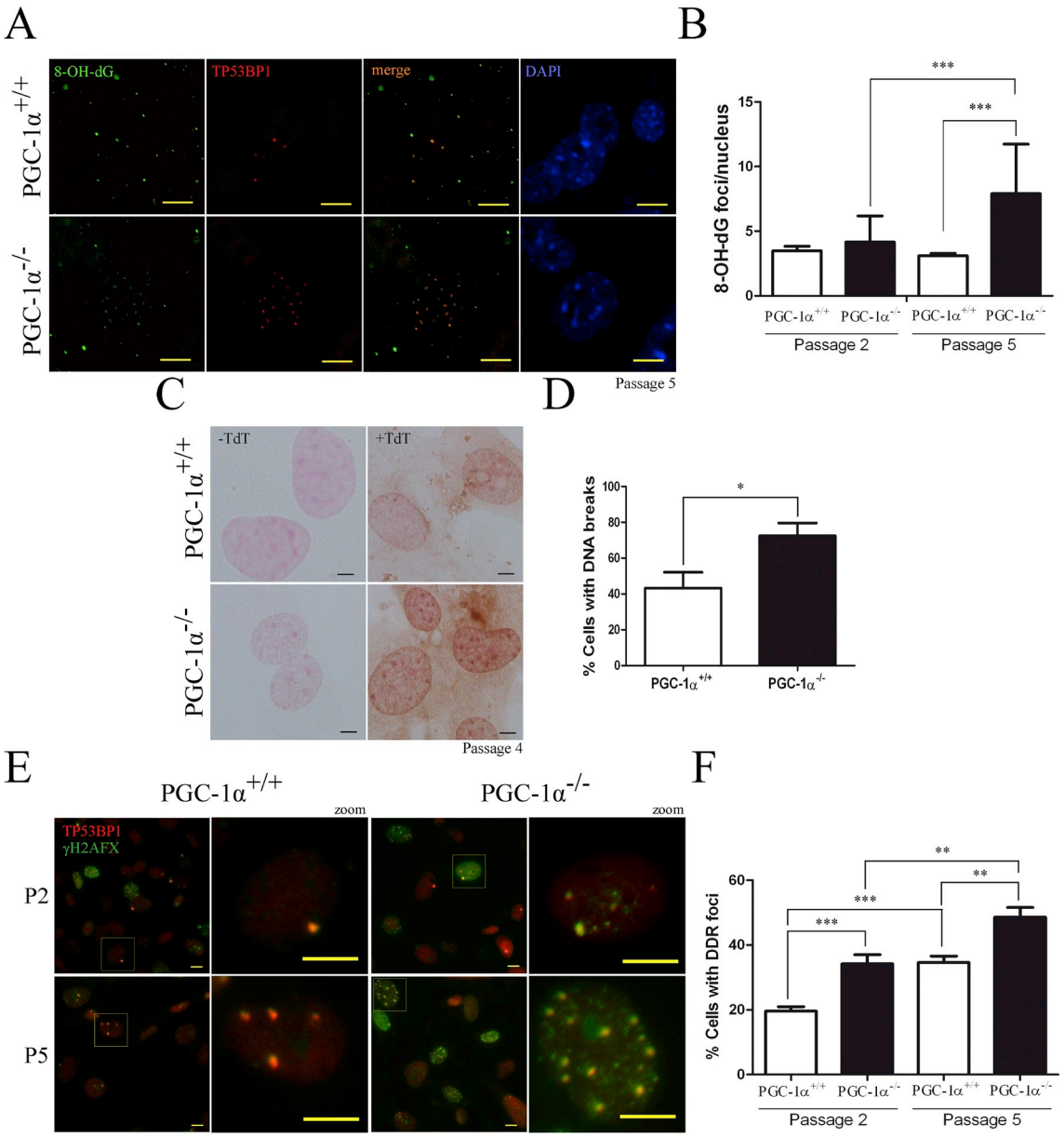

Fig. 2. PGC-1α-deficient MEFs show increased levels of oxidative DNA damage and double-strand breaks. **A)** Representative immunofluorescence images of PGC-1α$^{+/+}$ and PGC-1α$^{-/-}$ MEFs showing TP53BP1/8-OH-dG nuclear *foci* (100 ×). Scale bar, 10 μm. **B)** Quantitative analysis of 8-OH-dG nuclear *foci*. **C)** Representative immunohistochemistry images of PGC-1α$^{+/+}$ and PGC-1α$^{-/-}$ MEFs showing DNA strand breaks labeled with biotinylated dUTP and TdT (60 ×). Scale bar, 10 μm. **D)** Quantitative analysis of DNA strand breaks. **E)** Representative imunoflorescence images of PGC-1α$^{+/+}$ and PGC-1α$^{-/-}$ MEFs showing TP53BP1/γH2AFX *foci* (40 ×). Scale bar, 10 μm. **F)** Quantitative analysis of TP53BP1/γH2AFX *foci* (DDR *foci*). Data represent the means ± SD, n = 3 independent cultures *, $p \leq 0.05$; **, $p \leq 0.01$; ***, $p \leq 0.005$. n = 3.

gal-positive cells were higher for PGC-1α$^{-/-}$ MEFs than for PGC-1α$^{+/+}$ MEFs from p3, and this was statistically significant at p6. When cell cultures stopped growing, 47% of PGC-1α$^{-/-}$ MEFs and 31% of PGC-1α$^{+/+}$ MEFs were β-gal-positive (Fig. 4A and B).

As noted earlier, ROS and DNA damage induced premature senescence and cell cycle arrest depends on the activation/induction of at least two key cell cycle regulators, p53 and p16. Other important factors include the CDK inhibitors p19 and p21, which are direct targets of p53, and widely used as senescence and cell cycle arrest markers. Thus, we monitored total and phosphorylated levels p53 as well as p16, p19 and p21 mRNA and protein levels by western blotting of MEF cell lysates at different cell passages. In accord with the earlier induction of SA-β-gal activity, the levels of p53 phosphorylation were higher at early passages in PGC-1α$^{-/-}$ MEFs than in PGC-1α$^{+/+}$ MEFs (Fig. 4C). Similarly, mRNA and protein levels of both p16 and p19, as well as p21 protein levels, were higher at early passages in PGC-1α$^{-/-}$ MEFs than in PGC-1α$^{+/+}$ MEFs (Fig. 4D). These results are consistent with the induction of premature senescence (Fig. 4C and D). Representative western blots can be found in Supp. Fig. 7.

3.5. Early senescence escape of PGC-1α-deficient MEFs

Despite the evident early induction of senescence markers in PGC-1α-deficient MEFs, cell proliferation rates were not significantly different between PGC-1α$^{+/+}$ and PGC-1α$^{-/-}$ cultures. Population doubling levels decreased with each passage in both cell types at similar rates and cultures reached senescence at the same time, cell cultures did not proliferate after 20 days in culture (Fig. 5A and B). In fact, immortalization occurred significantly sooner for PGC-1α$^{-/-}$ MEFs. Accordingly, PGC-1α$^{-/-}$ MEFs immortalized on average after 9 days of

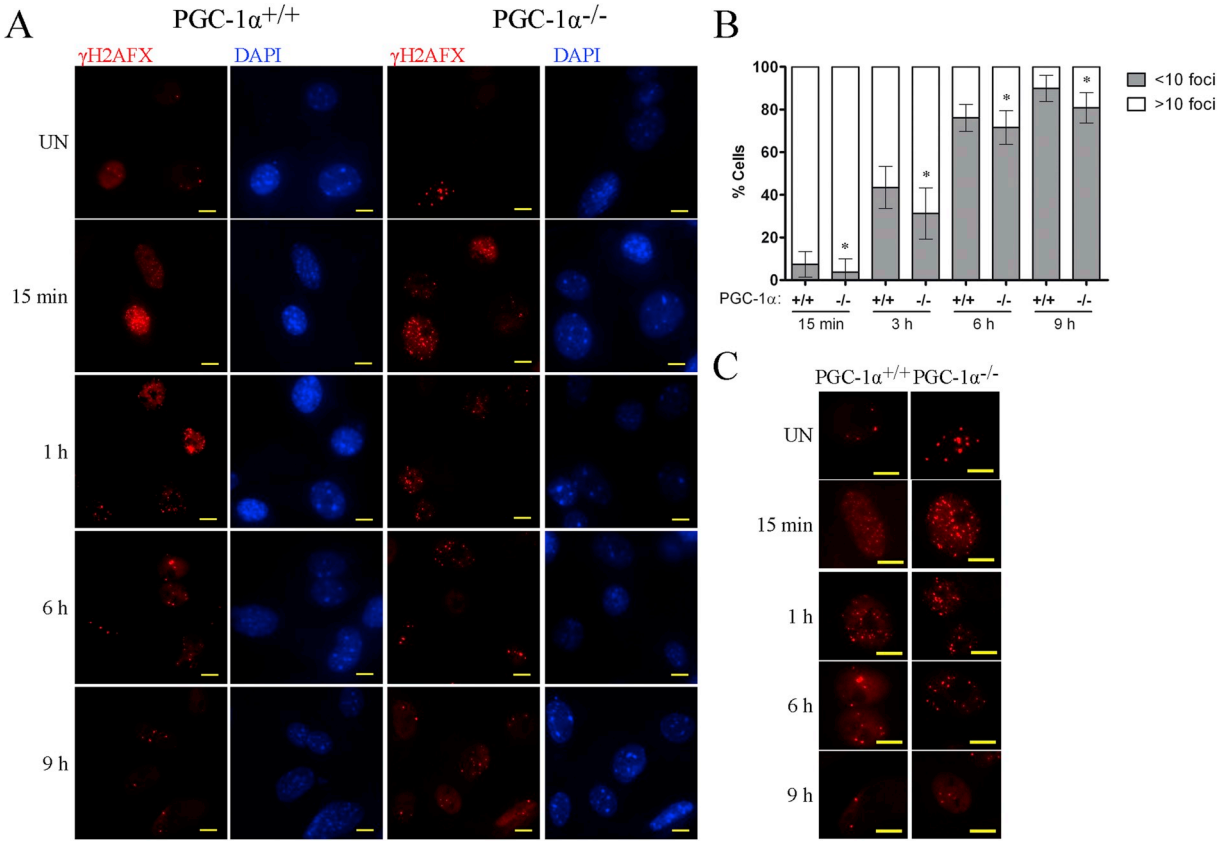

Fig. 3. Evaluation of DNA damage repair. **A)** Representative immunofluorescence images of PGC-1α$^{+/+}$ and PGC-1α$^{-/-}$ MEFs showing DDR *foci* (γH2AFX) at different times following 3 Gy irradiation. Untreated (UN). Scale bar, 10 μm. **B)** Graph shows the % of cells with > 10 DDR *foci* and < 10 DDR *foci*. **C)** Zoom-in images of PGC-1α$^{+/+}$ and PGC-1α$^{-/-}$ MEFs showing DDR *foci*. Untreated (UN). Scale bar, 10 μm. Data represent the means ± SD, n = 3 independent cell cultures. * $p < 0.05$. The statistical analysis for the figure compares for the contrast WT vs KO at each time point the relative % distribution of cells with more or less than 10 foci per nucleus using paired T test $p \leq 0.05$, for the comparison of $+/+$ vs $-/-$ MEFs at each of the indicated time points.

senescence, whereas this occurred on average after 26 days for PGC-1α$^{+/+}$ MEFs. Following immortalization, PGC-1α$^{+/+}$ and PGC-1α$^{-/-}$ MEFs again proliferated at similar rates (Fig. 5C). This result suggests that the induction of p53 and the upregulation of CDK inhibitors in PGC-1α$^{-/-}$ MEFs was insufficient to adequately arrest cell proliferation.

3.6. Differential expression of p53 target genes in PGC-1α deficient MEFs

PGC-1α has been shown to directly interact and regulate p53 transcriptional activity [28]. We therefore questioned whether the observed impairment of cell cycle inhibition and early senescence escape in PGC-1α$^{-/-}$ MEFs could be due to a blunted induction of p53 target genes. To test this hypothesis, we analyzed the expression of a panel of p53-regulated genes: the pro-apoptotic proteins *bax*, *bbc3 (puma)* and *pmaip1 (noxa)*; the oxidative stress cell cycle regulators *sesn1*, *sesn2*, *ndn (necdin)* and *gadd45a*, the metabolic enzymes *gls2* or *aldh4, terc (telomerase RNA component) and park2 (parkin gene encoding an E3 ubiquitin ligase)*. The mRNA levels of *sesn2*, *puma*, noxa, *aldh4*, *terc* and *necdin* were significantly lower in PGC-1α$^{-/-}$ MEFs than in PGC-1α$^{+/+}$ MEFs while the others showed a similar tendency (Fig. 6). This general decrease in the expression of p53 target genes suggests an attenuated p53 transcriptional activity in PGC-1α$^{-/-}$ MEFs and is consistent with the observed loss of cell growth arrest in the face of elevated DNA damage and early immortalization.

4. Discussion

The mechanisms that induce and control cellular senescence have been thoroughly investigated [47]and it is well established that ROS trigger oxidative DNA damage [48] and senescence [49]. While the induction of a senescence-like phenotype is currently considered a feasible cancer therapy approach [50], whether it is friend or foe in tumor development remains contentious [51] and raises the question of whether it prevents immortalization or is the stage that precedes it. The link between metabolic dysfunction observed in a significant proportion of the world's population [52] and the noted higher risk of tumor development [53] is also a focus of intense scientific debate since oxidative metabolism has been also shown to be associated with resistance to cancer treatments [54]. In the present study, we show that PGC-1α, a master regulator of mitochondrial function and ROS control [22] whose expression is down-regulated by feeding [55], plays an important role in replicative senescence since in its absence the consequent elevated ROS levels are associated with increased levels of DNA oxidation and DNA damage. However, cell cycle control mechanisms fail, possibly due to reduced p53 activity, promoting *de facto* immortalization.

We first examined how serial passage of MEFs modified PGC-1α target gene expression. Expression of the antioxidant MnSOD gradually declined following consecutive cell passages. In a background of PGC-1α deficiency, MEFs showed reduced levels of MnSOD and the passage-dependent loss of expression was less marked than in equivalent wild-type cells, suggesting this is at least partially dependent on PGC-1α. PGC-1α deficiency in MEFs was accompanied by the increased production of mitochondrial ROS and, as expected, ROS production was significantly higher in PGC-1α$^{-/-}$ MEFs than in PGC-1α$^{+/+}$ MEFs from passage 3. Remarkably, the passage-dependent increase in ROS production in PGC-1α$^{-/-}$ MEFs was more marked than that in PGC-1α$^{+/+}$ MEFs, possibly reflecting the well-characterized damaging effect of ROS on mitochondrial function, which renders mitochondria even more

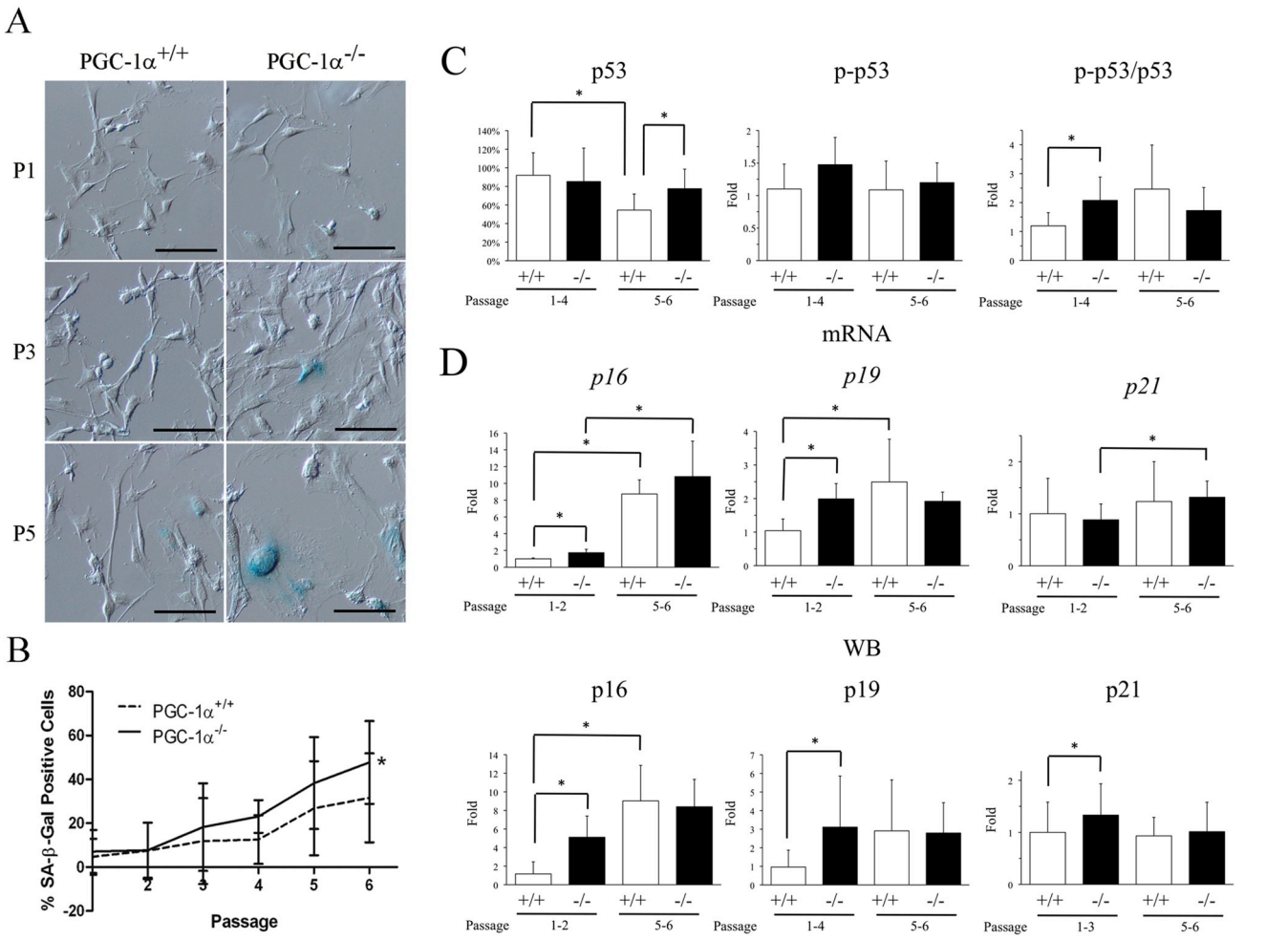

Fig. 4. PGC-1α-deficient MEFs present early senescence markers. **A)** Representative images of β-galactosidase staining in PGC-1α$^{+/+}$ and PGC-1α$^{-/-}$ MEFs (10 ×). Scale bar, 100 μm. **B)** Quantification of cells positive for senescence-associated β-galactosidase activity. **C)** Western blot analysis of p53 (total and phosphorylated at Ser 15), in serially-passaged PGC-1α$^{+/+}$ and PGC-1α$^{-/-}$ MEFs. β-actin was used as a loading control. **D)** qPCR mRNA and western blot analysis of p16, p19 and p21 in serially-passaged PGC-1α$^{+/+}$ and PGC-1α$^{-/-}$ MEFs. β-actin was used as a loading control. Data for PGC-1α$^{+/+}$ MEFs at passage 1 were assigned a value of 1 or 100%. Data represent the means ± SD. The graph shows the average values for the indicated passages. Selected passage ranges are those within which the values did not change significantly. n = 4 independent cell cultures. *, p≤0.05; ***, p ≤ 0,005.

dysfunctional and "ROS-genic".

We next evaluated the impact of elevated ROS production for DNA oxidation and genomic instability. Consistent with the elevated levels of ROS, we observed higher levels of DNA oxidation and DSBs in PGC-1α$^{-/-}$ MEFs. We ruled out the possibility that the increase in DSBs was associated with an impaired DNA repair system since direct evaluation of the induction of DNA repair activities using γ-radiation showed only a marginal defect in PGC-1α$^{-/-}$ MEFs, which is not likely to be the mechanism behind the observed levels of DSBs in serially-passaged cells.

Considering that both elevated ROS levels and DNA damage can induce senescence mediators that inhibit cell cycle progression, we monitored the activation of p53 and the induction of p16 and p19, consistently finding an early activation of these senescence mediators in PGC-1α$^{-/-}$ MEFs. However, cell proliferation rates were not significantly different between PGC-1α$^{+/+}$ and PGC-1α$^{-/-}$ MEFs, suggesting that downstream mediators of cell proliferation were not efficiently induced. Furthermore, PGC-1α$^{-/-}$ MEFs immortalization was significantly faster, possibly suggesting a failure to adequately induce cell death. In PGC-1α$^{+/+}$ cells the ratio p-p53/p53 was higher in "late" passages than in "early" passages as previously described. It is possible that in PGC-1α$^{-/-}$ cells since the damage occurs earlier, there is an earlier activation of p53, and that could explain why the ratio p-p53/p53 at "early" passages is higher in PGC-1α$^{-/-}$ than in PGC-1α$^{+/+}$ MEFs. To elucidate why the p-p53/p53 ratio is not further enhanced in PGC-1α$^{-/-}$ MEFs at "late" passages despite of the evident increase in DNA damage deserves further investigation.

Taking into account that p53 plays a key role both in cell cycle arrest and ROS-induced apoptotic cell death [56], and that PGC-1α can operate as a coactivator of p53 transcriptional activity [28], we evaluated the expression levels of a panel of p53 target genes including inductors of cell cycle arrest and apoptosis. We found that the levels of several of these genes were significantly lower in PGC-1α$^{-/-}$ MEFs, despite the observed moderate increase in activated p53 in these cells, possibly suggesting that the failure to properly induce cell cycle arrest and pro-apoptotic gene expression may facilitate the immortalization of PGC-1α$^{-/-}$ MEFs. Additionally, the observation that the induction of p21 levels (another p53 target, and cell cycle inhibitor) in PGC-1α$^{-/-}$ MEFs at "late" passages is smaller than what should be expected taking into account the level of DNA damage in these cells, also argue in favor of a p53 dependent mechanism.

Still, one limitation of the study is that the nature of the mutations occurring in PGC-1α$^{+/+}$ and PGC-1α$^{-/-}$ MEFs leading to immortalization has not been tested. Also, the causality of the increased levels of superoxide in PGC-1α on DNA damage could not be evaluated since antioxidant treatments per se alter the cell cycle due to the role

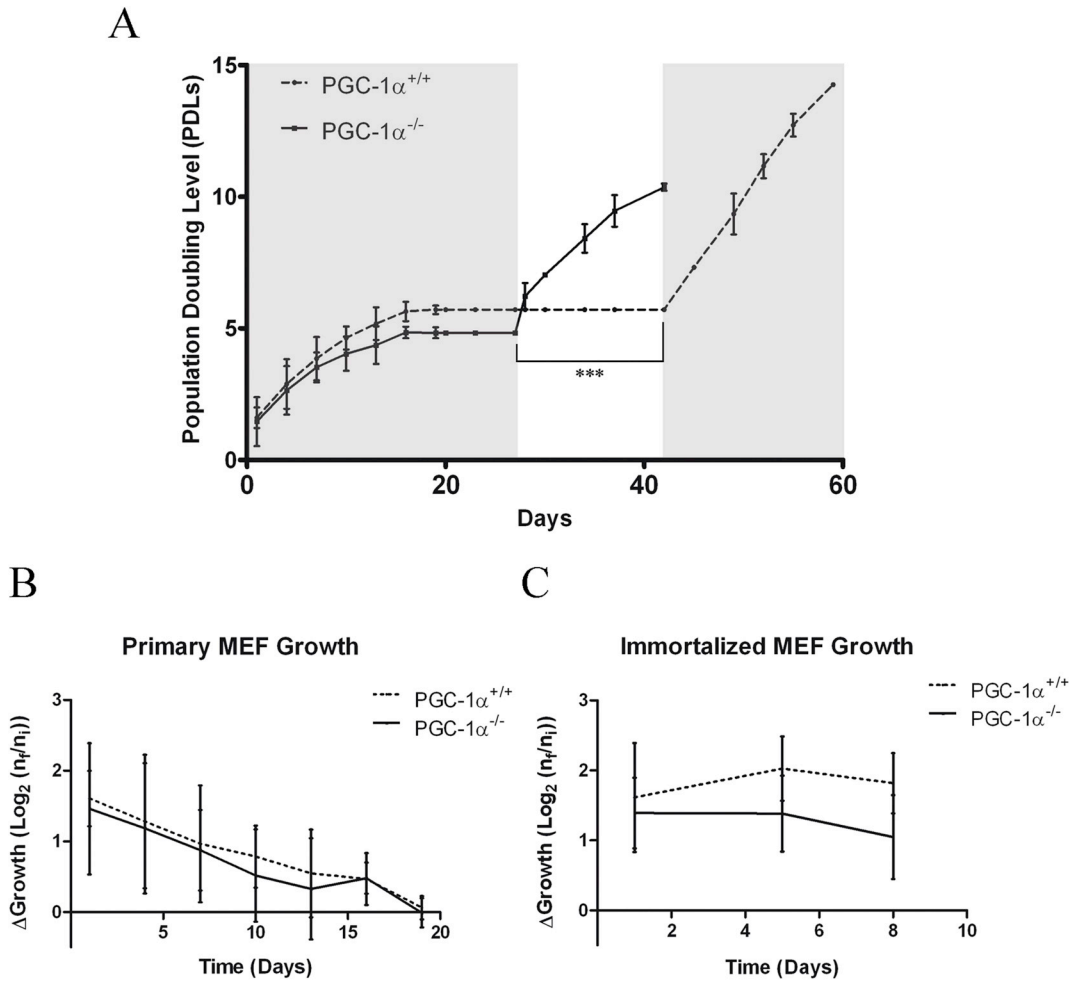

Fig. 5. Growth rates, senescence arrest and escape of wild-type and PGC-1α-deficient MEFs. **A)** Population doubling level rates were calculated with the formula $\Delta Growth = Log_2 (n_f/n_i)$; where n_i is the number of cells plated and n_f is the number of cells before the next passage. The white background section indicates the difference in immortalization rates. **B)** Primary MEF growth rates. **C)** Immortalized MEF growth rates. Data represent the means ± SD, n = 8 independent cell cultures. ***, $p \leq 0.005$.

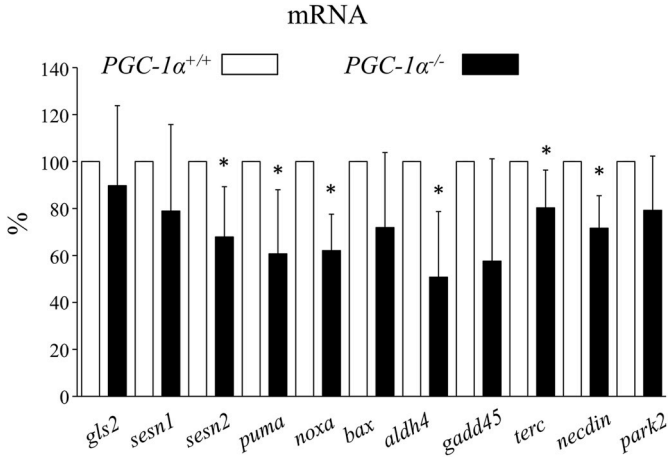

Fig. 6. qRT-PCR analysis of mRNA levels of p53 target genes in wild-type and PGC-1α-deficient MEFs at passage 5. Wild-type samples were assigned the value of 100%. Data are means ± SD of passages 1–6. n = 4 independent cell cultures. *, $p < 0.05$.

the cellular redox status plays in its control.

PGC-1α is recognized as a master regulator of mitochondrial function, including the control of mitochondrial ROS production. The long noted metabolic shift associated with tumor development, the Warburg effect, that makes cancer cell predominantly glycolytic has [57] fostered investigation on the possible role of PGC-1α in tumor development. While some studies attribute to PGC-1α a predominant tumor suppressor role preventing, for example, prostate cancer tumor metastasis [58], others find just the opposite in breast cancer [59], making it necessary further studies to define the molecular and functional basis for these differences. Our results highlight a novel aspect of how PGC-1α could impact tumor development by promoting ROS-induced DNA damage and early immortalization, possibly fostered by a defective activation of p53 and the senescence program.

Conflicts of interest

None declared.

Acknowledgements

This work was supported by grants from the Spanish Ministerio de Economía Industria y Competitividad (MINEICO) and FEDER funds [Grant numbers SAF2012-37693, SAF2015-63904-R, SAF2015-71521-REDC, to M.M., BFU-2014-53610-P to A.A.], from the European Union's Horizon 2020 research and innovation programme under the Marie Skłodowska-Curie Action grant agreement 721236-TREATMENT to M.M. and MPY-1038/14 and MPY-1146/16 from ISCIII to A.Z.

Appendix A. Supplementary data

Supplementary data to this article can be found online at https://doi.org/10.1016/j.freeradbiomed.2019.04.015.

List of Abbreviations

(ATM) Ataxia-telangiectasia mutated kinase
(SA-β-gal) β-galactosidase
(CDK) Cyclin dependent kinase
(cyt *c*) Cytochrome C
(DD) DNA damage
(DDR) DNA damage repair
(DSB) Double strand break
(DMEM) Dulbecco's modified Eagle's medium
(FBS) Fetal bovine serum
(IF) Immunofluorescence
(IHQ) Immunohistochemistry
(LATS1) Large tumor suppressor kinase 1
(ETC) Mitochondrial electron transport chain
(MnSOD) Mn superoxide dismutase
(MEF) Mouse embryonic fibroblast
(NHEJ) Non-homologous end-joining
(8-OH-dG) 8-oxo-deoxyguanosine
(P) Passage
(PGC-1α) Peroxisome proliferator activated receptor γ co-activator 1α
(γH2AFX) Phosphorylated histone H2AFX
(PDLs) Population doubling level
(ROS) Reactive oxygen species
(TdT) Terminal transferase
(WB) Western blotting

References

[1] T. Kuilman, C. Michaloglou, W.J. Mooi, D.S. Peeper, The essence of senescence, Genes Dev. 24 (2010) 2463–2479.
[2] A. Bernadotte, V.M. Mikhelson, I.M. Spivak, Markers of cellular senescence. Telomere shortening as a marker of cellular senescence, Aging (Albany NY) 8 (2016) 3–11.
[3] U.K. Rajarajacholan, K. Riabowol, Aging with ING: a comparative study of different forms of stress induced premature senescence, Oncotarget 6 (2015) 34118–34127.
[4] C. Chandeck, W.J. Mooi, Oncogene-induced cellular senescence, Adv. Anat. Pathol. 17 (2010) 42–48.
[5] I. Fridlyanskaya, L. Alekseenko, N. Nikolsky, Senescence as a general cellular response to stress: a mini-review, Exp. Gerontol. 72 (2015) 124–128.
[6] R. Colavitti, T. Finkel, Reactive oxygen species as mediators of cellular senescence, IUBMB Life 57 (2005) 277–281.
[7] E. Panieri, V. Gogvadze, E. Norberg, R. Venkatesh, S. Orrenius, B. Zhivotovsky, Reactive oxygen species generated in different compartments induce cell death, survival, or senescence, Free Radic. Biol. Med. 57 (2013) 176–187.
[8] E. Samper, D.G. Nicholls, S. Melov, Mitochondrial oxidative stress causes chromosomal instability of mouse embryonic fibroblasts, Aging Cell 2 (2003) 277–285.
[9] G. Saretzki, M.P. Murphy, T. von Zglinicki, MitoQ counteracts telomere shortening and elongates lifespan of fibroblasts under mild oxidative stress, Aging Cell 2 (2003) 141–143.
[10] Y. Johmura, M. Nakanishi, Multiple facets of p53 in senescence induction and maintenance, Cancer Sci. 107 (2016) 1550–1555.
[11] H. Rayess, M.B. Wang, E.S. Srivatsan, Cellular senescence and tumor suppressor gene p16, Int. J. Cancer 130 (2012) 1715–1725.
[12] J. Campisi, F. d'Adda di Fagagna, Cellular senescence: when bad things happen to good cells, Nat. Rev. Mol. Cell Biol. 8 (2007) 729–740.
[13] D. Liu, Y. Xu, p53, oxidative stress, and aging, Antioxidants Redox Signal. 15 (2011) 1669–1678.
[14] N.C. Jenkins, T. Liu, P. Cassidy, S.A. Leachman, K.M. Boucher, A.G. Goodson, G. Samadashwily, D. Grossman, The p16(INK4A) tumor suppressor regulates cellular oxidative stress, Oncogene 30 (2011) 265–274.
[15] A.B. Williams, B. Schumacher, p53 in the DNA-Damage-Repair Process, Cold Spring Harb Perspect Med 6 (2016).
[16] A. Takahashi, N. Ohtani, K. Yamakoshi, S. Iida, H. Tahara, K. Nakayama, K.I. Nakayama, T. Ide, H. Saya, E. Hara, Mitogenic signalling and the p16INK4a-Rb pathway cooperate to enforce irreversible cellular senescence, Nat. Cell Biol. 8 (2006) 1291–1297.
[17] M. Lee, J.S. Lee, Exploiting tumor cell senescence in anticancer therapy, BMB Rep 47 (2014) 51–59.
[18] P. Francica, D.M. Aebersold, M. Medova, Senescence as biologic endpoint following pharmacological targeting of receptor tyrosine kinases in cancer, Biochem. Pharmacol. 126 (2017) 1–12.
[19] C.H. Chan, Y. Gao, A. Moten, H.K. Lin, Novel ARF/p53-independent senescence pathways in cancer repression, J. Mol. Med. (Berl.) 89 (2011) 857–867.
[20] S. Chakradeo, L.W. Elmore, D.A. Gewirtz, Is senescence reversible? Curr. Drug Targets 17 (2016) 460–466.
[21] C. Canto, J. Auwerx, PGC-1alpha, SIRT1 and AMPK, an energy sensing network that controls energy expenditure, Curr. Opin. Lipidol. 20 (2009) 98–105.
[22] I. Valle, A. Alvarez-Barrientos, E. Arza, S. Lamas, M. Monsalve, PGC-1alpha regulates the mitochondrial antioxidant defense system in vascular endothelial cells, Cardiovasc. Res. 66 (2005) 562–573.
[23] M.E. Patti, A.J. Butte, S. Crunkhorn, K. Cusi, R. Berria, S. Kashyap, Y. Miyazaki, I. Kohane, M. Costello, R. Saccone, E.J. Landaker, A.B. Goldfine, E. Mun, R. DeFronzo, J. Finlayson, C.R. Kahn, L.J. Mandarino, Coordinated reduction of genes of oxidative metabolism in humans with insulin resistance and diabetes: potential role of PGC1 and NRF1, Proc. Natl. Acad. Sci. U. S. A. 100 (2003) 8466–8471.
[24] R.K. Semple, V.C. Crowley, C.P. Sewter, M. Laudes, C. Christodoulides, R.V. Considine, A. Vidal-Puig, S. O'Rahilly, Expression of the thermogenic nuclear hormone receptor coactivator PGC-1alpha is reduced in the adipose tissue of morbidly obese subjects, Int. J. Obes. Relat. Metab. Disord. 28 (2004) 176–179.
[25] X. Yang, S. Enerback, U. Smith, Reduced expression of FOXC2 and brown adipogenic genes in human subjects with insulin resistance, Obes. Res. 11 (2003) 1182–1191.
[26] M. Aharoni-Simon, M. Hann-Obercyger, S. Pen, Z. Madar, O. Tirosh, Fatty liver is associated with impaired activity of PPARgamma-coactivator 1alpha (PGC1alpha) and mitochondrial biogenesis in mice, Lab. Invest. 91 (2011) 1018–1028.
[27] E. Barroso, R. Rodriguez-Calvo, L. Serrano-Marco, A.M. Astudillo, J. Balsinde, X. Palomer, M. Vazquez-Carrera, The PPARbeta/delta activator GW501516 prevents the down-regulation of AMPK caused by a high-fat diet in liver and amplifies the PGC-1alpha-Lipin 1-PPARalpha pathway leading to increased fatty acid oxidation, Endocrinology 152 (2011) 1848–1859.
[28] N. Sen, Y.K. Satija, S. Das, PGC-1alpha, a key modulator of p53, promotes cell survival upon metabolic stress, Mol. Cell 44 (2011) 621–634.
[29] S. Xiong, N. Patrushev, F. Forouzandeh, L. Hilenski, R.W. Alexander, PGC-1alpha modulates telomere function and DNA damage in protecting against aging-related chronic diseases, Cell Rep. 12 (2015) 1391–1399.
[30] S. Xiong, G. Salazar, N. Patrushev, M. Ma, F. Forouzandeh, L. Hilenski, R.W. Alexander, Peroxisome proliferator-activated receptor gamma coactivator-1alpha is a central negative regulator of vascular senescence, Arterioscler. Thromb. Vasc. Biol. 33 (2013) 988–998.
[31] C. Sanchez-Ramos, A. Tierrez, O. Fabregat-Andres, B. Wild, F. Sanchez-Cabo, A. Arduini, A. Dopazo, M. Monsalve, PGC-1alpha regulates translocated in liposarcoma activity: role in oxidative stress gene expression, Antioxidants Redox Signal. 15 (2011) 325–337.
[32] P. Sancho, E. Burgos-Ramos, A. Tavera, T. Bou Kheir, P. Jagust, M. Schoenhals, D. Barneda, K. Sellers, R. Campos-Olivas, O. Grana, C.R. Viera, M. Yuneva, B. Sainz Jr., C. Heeschen, MYC/PGC-1alpha balance determines the metabolic phenotype and plasticity of pancreatic cancer stem cells, Cell Metabol. 22 (2015) 590–605.
[33] Y. Olmos, I. Valle, S. Borniquel, A. Tierrez, E. Soria, S. Lamas, M. Monsalve, Mutual dependence of Foxo3a and PGC-1alpha in the induction of oxidative stress genes, J. Biol. Chem. 284 (2009) 14476–14484.
[34] A. Zambrano, V. Garcia-Carpizo, M.E. Gallardo, R. Villamuera, M.A. Gomez-Ferreria, A. Pascual, N. Buisine, L.M. Sachs, R. Garesse, A. Aranda, The thyroid hormone receptor beta induces DNA damage and premature senescence, J. Cell Biol. 204 (2014) 129–146.
[35] S. Borniquel, N. Garcia-Quintans, I. Valle, Y. Olmos, B. Wild, F. Martinez-Granero, E. Soria, S. Lamas, M. Monsalve, Inactivation of Foxo3a and subsequent downregulation of PGC-1 alpha mediate nitric oxide-induced endothelial cell migration, Mol. Cell Biol. 30 (2010) 4035–4044.
[36] K.M. Robinson, M.S. Janes, J.S. Beckman, The selective detection of mitochondrial superoxide by live cell imaging, Nat. Protoc. 3 (2008) 941–947.
[37] M. Monsalve, Z. Wu, G. Adelmant, P. Puigserver, M. Fan, B.M. Spiegelman, Direct coupling of transcription and mRNA processing through the thermogenic coactivator PGC-1, Mol. Cell 6 (2000) 307–316.
[38] G.J. Todaro, H. Green, Quantitative studies of the growth of mouse embryo cells in culture and their development into established lines, J. Cell Biol. 17 (1963) 299–313.
[39] J. Cadet, T. Douki, J.L. Ravanat, Oxidatively generated base damage to cellular DNA, Free Radic. Biol. Med. 49 (2010) 9–21.
[40] O.A. Sedelnikova, C.E. Redon, J.S. Dickey, A.J. Nakamura, A.G. Georgakilas, W.M. Bonner, Role of oxidatively induced DNA lesions in human pathogenesis, Mutat. Res. 704 (2010) 152–159.
[41] N.C. Bauer, A.H. Corbett, P.W. Doetsch, The current state of eukaryotic DNA base damage and repair, Nucleic Acids Res. 43 (2015) 10083–10101.
[42] M. Shrivastav, L.P. De Haro, J.A. Nickoloff, Regulation of DNA double-strand break repair pathway choice, Cell Res. 18 (2008) 134–147.
[43] S. Panier, S.J. Boulton, Double-strand break repair: 53BP1 comes into focus, Nat. Rev. Mol. Cell Biol. 15 (2014) 7–18.
[44] E.P. Rogakou, D.R. Pilch, A.H. Orr, V.S. Ivanova, W.M. Bonner, DNA double-stranded breaks induce histone H2AX phosphorylation on serine 139, J. Biol. Chem. 273 (1998) 5858–5868.
[45] N. Dimitrova, Y.C. Chen, D.L. Spector, T. de Lange, 53BP1 promotes non-homologous end joining of telomeres by increasing chromatin mobility, Nature 456 (2008) 524–528.
[46] Y.M. Chung, S.B. Lee, H.J. Kim, S.H. Park, J.J. Kim, J.S. Chung, Y.D. Yoo,

Replicative senescence induced by Romo1-derived reactive oxygen species, J. Biol. Chem. 283 (2008) 33763–33771.
[47] S. He, N.E. Sharpless, Senescence in Health and disease, Cell 169 (2017) 1000–1011.
[48] J. Cadet, J.R. Wagner, DNA base damage by reactive oxygen species, oxidizing agents, and UV radiation, Cold Spring Harb Perspect Biol 5 (2013).
[49] A. Chandrasekaran, M. Idelchik, J.A. Melendez, Redox control of senescence and age-related disease, Redox Biol 11 (2017) 91–102.
[50] R. Leite de Oliveira, R. Bernards, Anti-cancer therapy: senescence is the new black, EMBO J. 37 (2018).
[51] M. Schosserer, J. Grillari, M. Breitenbach, The dual role of cellular senescence in developing tumors and their response to cancer therapy, Front Oncol 7 (2017) 278.
[52] A. Engin, The definition and prevalence of obesity and metabolic syndrome, Adv. Exp. Med. Biol. 960 (2017) 1–17.
[53] S.S. Doerstling, C.H. O'Flanagan, S.D. Hursting, Obesity and cancer metabolism: a perspective on interacting tumor-intrinsic and extrinsic factors, Front Oncol 7 (2017) 216.
[54] C. Bosc, M.A. Selak, J.E. Sarry, Resistance is futile: targeting mitochondrial energetics and metabolism to overcome drug resistance in cancer treatment, Cell Metabol. 26 (2017) 705–707.
[55] H. Liang, W.F. Ward, PGC-1alpha: a key regulator of energy metabolism, Adv. Physiol. Educ. 30 (2006) 145–151.
[56] J. Chen, The cell-cycle arrest and apoptotic functions of p53 in tumor initiation and progression, Cold Spring Harb Perspect Med 6 (2016) a026104.
[57] M. Zdralevic, M. Vucetic, B. Daher, I. Marchiq, S.K. Parks, J. Pouyssegur, Disrupting the 'Warburg effect' re-routes cancer cells to OXPHOS offering a vulnerability point via 'ferroptosis'-induced cell death, Adv Biol Regul 68 (2018) 55–63.
[58] V. Torrano, L. Valcarcel-Jimenez, A.R. Cortazar, X. Liu, J. Urosevic, M. Castillo-Martin, S. Fernandez-Ruiz, G. Morciano, A. Caro-Maldonado, M. Guiu, P. Zuniga-Garcia, M. Graupera, A. Bellmunt, P. Pandya, M. Lorente, N. Martin-Martin, J.D. Sutherland, P. Sanchez-Mosquera, L. Bozal-Basterra, A. Zabala-Letona, A. Arruabarrena-Aristorena, A. Berenguer, N. Embade, A. Ugalde-Olano, I. Lacasa-Viscasillas, A. Loizaga-Iriarte, M. Unda-Urzaiz, N. Schultz, A.M. Aransay, V. Sanz-Moreno, R. Barrio, G. Velasco, P. Pinton, C. Cordon-Cardo, J.W. Locasale, R.R. Gomis, A. Carracedo, The metabolic co-regulator PGC1alpha suppresses prostate cancer metastasis, Nat. Cell Biol. 18 (2016) 645–656.
[59] S. Andrzejewski, E. Klimcakova, R.M. Johnson, S. Tabaries, M.G. Annis, S. McGuirk, J.J. Northey, V. Chenard, U. Sriram, D.J. Papadopoli, P.M. Siegel, J. St-Pierre, PGC-1alpha promotes breast cancer metastasis and confers bioenergetic flexibility against metabolic drugs, Cell Metabol. 26 (2017) 778–787 e775.
[60] M. Gardiner, R. Toth, F. Vandermoere, N.A. Morrice, J. Rouse, Identification and characterization of FUS/TLS as a new target of ATM, Biochem. J. 415 (2008) 297–307, https://doi.org/10.1042/BJ20081135.